DEU FMD 26(76) (2024) 156-166

Dokuz Eylül Üniversitesi Mühendislik Fakültesi Fen ve Mühendislik Dergisi
Dokuz Eylul University Faculty of Engineering Journal of Science and Engineering
Elektronik/Online ISSN: 2547-958X

RESEARCH ARTICLE / ARAŞTIRMA MAKALESI

Estimation of Fault Parameters in Southwest of the Thrace Basin from Gravity Gradient Data

Trakya Havzasının Güneybatısında Fay Parametrelerinin Gravite Gradyent Verilerinden Kestirimi

Sibel Uzun

Ondokuz Mayıs Üniversitesi, Mühendislik Fakültesi, Harita Mühendisliği Bölümü, Samsun, TÜRKİYE
Corresponding Author / Sorumlu Yazar *: sibel.uzun@omu.edu.tr

Abstract

Characterization of fault zones plays an important role for earthquake studies, geothermal and mineral resource exploration. This problem can be achieved by optimizing parameters of a defined synthetic model iteratively using gravity, gravity gradients or magnetic data. Curvature gradients indicate deviations of an equipotential surface from a spherical surface, therefore, reflecting deviations of mass distributions from a source point. In this study, differential curvature gradient is used as it identifies linear structures such as dip-slip faults and geological contacts. Curvature gradients are computed from gravity gradient observations which are derived from the high-resolution Earth Gravitational Model 2008. Estimating the fault parameters from gravity gradients is a complex nonlinear geophysical inverse problem that requires finding the minimum of a multi-variable cost function. A global optimization technique called simulated annealing (SA) is used to estimate location, dip angle and some depth parameters of the faults located in southwest side of the Thrace basin in Türkiye. In the optimization technique, a straight solution is inevitably applied to calculate the theoretical anomaly to be compared with the observed anomaly in each search step. In this case, the problem requires constructing a mathematical or geophysical interpretation model. Such a model is designed as a dip-slip fault model. The results show that dip angle estimates indicate high-angle faults which are found to be consistent with the seismic studies.

Keywords: *Gravity gradients, Simulated annealing, Fault parameters*

Öz

Fay zonlarının tanımlaması, deprem çalışmaları, jeotermal ve mineral kaynakların araştırılmasında önemli bir rol oynar. Bu problem tanımlanmış bir sentetik modelin parametrelerinin gravite, gravite gradyentleri ya da manyetik verilerden iteratif olarak optimize ederek çözülebilir. Eğrilik gradyentleri, bir eşpotansiyelli yüzeyin küresel bir yüzeyden sapmalarını ifade eder ve bu nedenle kütle dağılımlarının kaynak noktadan sapmalarını yansıtır. Bu çalışmada, eğim atımlı faylar ve jeolojik dokanaklar gibi doğrusal yapıları tanımlayan diferansiyel eğrilik gradyentleri kullanılmıştır. Eğrilik gradyentleri yüksek çözünürlüklü Yer Gravite Modeli 2008' den türetilen gravite gradyentlerinden hesaplanmıştır. Gravite gradyentlerinden fay parametrelerinin kestirimi çok değişkenli hata fonksiyonunun minimum değerini bulmayı gerektiren kompleks doğrusal olmayan bir jeofiziksel ters çözüm problemidir. Benzetimli tavlama olarak adlandırılan bir global optimizasyon yöntemi, Türkiyede Trakya havzasının güneybatısındaki fayların eğim açısı, konumu ve bazı derinlik parametrelerinin kestirimi için kullanılmıştır. Optimizasyon tekniğinde, her bir arama adımında gözlenen anomali ile karşılaştırılacak olan kuramsal anomaliyi hesaplamak için kaçınılmaz olarak düz çözüm de uygulanmaktadır. Bu durumda problem bir matematiksel veya jeofiziksel yorum modelinin kurgulanmasını gerektirir. Böyle bir model eğim atımlı fay modeli olarak tasarlanmıştır. Sonuçlar eğim açısı tahminlerinin sismik çalışmalarla uyumlu bulunan yüksek eğim açılı faylara işaret ettiğini göstermektedir.

Anahtar Kelimeler: *Gravite gradyanları, Benzetimli tavlama, Fay parametreleri*

1. Introduction

A triangular shape Thrace basin located in northwest side of Turkey is bordered by Strandja massif to the north, Rhodope massif to the west and Menderes massif to the south. Since the region is important for hydrocarbon and coal potential, many geological studies have been carried out from borehole, seismic and gravity data. [1] studied geometry of the faults in the northeast side of the basin and defined three major fault zones, Kirklareli, Babaeski and Lüleburgaz, mostly defined by strike-slip faults. These faults are characterized as a northern extend of the North Anatolian Fault Zone (NAFZ). [2] investigated basin development and hydrocarbon potential of the basin from well and seismic data. [3] investigated lignite potential of the basin. [4] investigated hydrocarbon potential of the northwest side of the basin using well and seismic data across strands of NAFZ. [5] studied stratigraphic model of the Thrace basin from well, seismic and outcrop data and provide sedimentary thickness map of the basin. [6] constructed 2D and 3D gravity model of the basin to investigate subsurface structures and geometry of the basin across the strike of the faults in northeast side of the basin. [7] firstly mapped faults in the southwestern of the Thrace basin and reported that the faults lying in this area include several normal faults and mostly strike-slip faults according to their field

DOI:10.21205/deufmd.2024267618

Atıf şekli / How to cite:
Uzun, S. (2024). Estimation of Fault Parameters in Southwest of the Thrace Basin from Gravity Gradient Data. DEUFMD, 26(76), 156-166.

Geliş Tarihi / Received: 13.03.2023
Kabul Tarihi / Accepted: 15.08.2023

observations. [8] have determined lineaments in the southwestern of the Thrace basin using Hough transform from gravity data.

While previous studies have focused on stratigraphy, geometry of the faults, structural and tectonic evolution to evaluate hydrocarbon potential from well and seismic data, this study focuses on estimating parameters of the faults located in southwestern of the Thrace basin from gravity gradients. To this end, curvature gradients have been used to identify linear structures masked in the gravity anomalies. Previously, [9] tried to estimate fault parameters from gravity data using genetic and particle swarm optimization in the region.

In this study, a Monte Carlo inversion technique called simulated annealing (SA) is used to estimate fault parameters such as dip angle, location and depth parameters. The purpose of the paper is to show that gravity gradients generated from EGM08 data is indicative of linear structures and these data can be inverted to estimate parameters related to fault geometry.

2. Materials and Methods

Estimation of the fault parameters from the gradients, a corresponding forward model needs be constructed. The fault model is defined as a horizontal dip-slip fault infinitely extended in the strike direction. Figure 1 shows the fault model and its parameters in a local (x-y-z) coordinate system. Here, the x-axis is orthogonal to the strike of the fault, the z-axis is defined in positive upward and the y-axis is parallel to the strike of the fault. The location parameter is defined with respect to a fixed origin where the fault plane intersects the Earth surface.

The observations are curvature gradients generated from Earth's gravitational model (EGM08). EGM08 is a spherical harmonic model of Earth's gravitational potential constructed from satellite, terrestrial, airborne gravity and satellite altimetry data. The model is complete to degree 2190 and order 2160. Its spatial resolution is about 9km at the equator [10].

Disturbing gravitational gradients are second order symmetric tensor of second order derivatives of disturbing potential. In a local cartesian coordinate system, the gradient disturbances are given by [11]

$$\Gamma = \begin{bmatrix} \Gamma_{xx} & \Gamma_{xy} & \Gamma_{xz} \\ \Gamma_{yx} & \Gamma_{yy} & \Gamma_{yz} \\ \Gamma_{zx} & \Gamma_{zy} & \Gamma_{zz} \end{bmatrix} = \begin{bmatrix} \frac{\partial^2 T}{\partial x^2} & \frac{\partial^2 T}{\partial x \partial y} & \frac{\partial^2 T}{\partial x \partial z} \\ \frac{\partial^2 T}{\partial y \partial x} & \frac{\partial^2 T}{\partial y^2} & \frac{\partial^2 T}{\partial y \partial z} \\ \frac{\partial^2 T}{\partial z \partial x} & \frac{\partial^2 T}{\partial z \partial y} & \frac{\partial^2 T}{\partial z^2} \end{bmatrix} \quad (1)$$

where the disturbing potential, T is defined as difference between actual gravity potential W and normal gravity potential U [12].

$$T = W - U \quad (2)$$

The unit of gradients are given in Eotvos, $1E = 1 \times 10^{-9} s^{-2}$. The sum of the diagonal elements of the gradient tensor Γ satisfies Laplace's equation in free space,

$$\Gamma_{xx} + \Gamma_{yy} + \Gamma_{zz} = 0 \quad (3)$$

The relation of the difference in radii of curvatures of an equipotential surface with differential curvature gradient is given by [13]

$$\Gamma_C = g_3 \left(\frac{1}{\zeta'_2} - \frac{1}{\zeta'_1} \right) = \sqrt{\left(\Gamma_{2,2} - \Gamma_{1,1}\right)^2 + \left(2\Gamma_{1,2}\right)^2} \quad (4)$$

where g_3 is vertical gravitational acceleration, ζ'_1 and ζ'_2 are minimum and maximum principal radii curvatures of the equipotential surface. Therefore, differential curvature gradient for the model is defined by

$$\Gamma_C = \sqrt{\left(\Gamma_{yy} - \Gamma_{xx}\right)^2 + \left(2\Gamma_{xy}\right)^2} \quad (5)$$

Since the y-axis is parallel to the strike of the fault, $\Gamma_{xy} = 0$ and $\Gamma_{yy} = 0$. From Laplace's equation, $\Gamma_{zz} = -\Gamma_{xx}$. Therefore, the resultant curvature gradient in equation 5 also becomes $\Gamma_C = |\Gamma_{zz}|$.

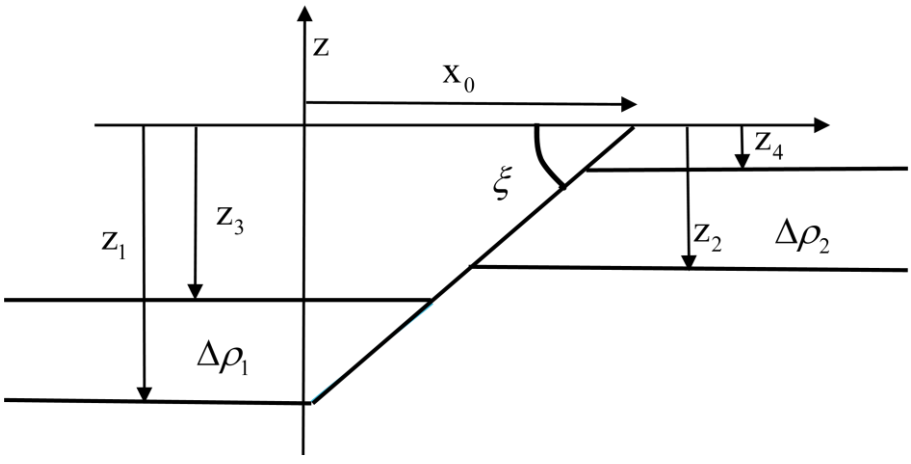

Figure 1. The geometrical representation for semi-infinite fault model. The fault parameters are the location, x_0 with respect to a fixed origin, the dip angle, χ, lower depth of left and right layers, z_1, z_2, upper depth of left and right layers, z_3, z_4 and density contrasts of left and right layers, $\Delta\rho_1$, $\Delta\rho_2$.

Here, the disturbing gravitational gradients are computed from EGM08 model. Spherical harmonic expansion of the disturbing potential T is given by (14)

$$T(r,\theta,\lambda) = \frac{GM}{a} \sum_{n=2}^{nmax} \left(\frac{a}{r}\right)^{n+1} \sum_{m=-n}^{n} \delta C_{nm} \overline{Y_{nm}}(\theta,\lambda) \quad (6)$$

where r, θ, λ is spherical polar coordinates, radius, co-latitude, longitude, respectively, GM is the product of Newton's gravitational constant and Earth's total mass, δC_{nm} is spherical harmonic coefficients being difference between coefficients for actual and normal gravitational potentials, a is the spherical radius being set to the semi-major axis of an Earth-fitting ellipsoid and $\overline{Y_{nm}}(\theta, \lambda)$ is surface spherical harmonics. Spherical polar coordinates, in terms of cartesian coordinates are expressed as [14]

$$\varphi = tan^{-1}\frac{z}{\sqrt{x^2+y^2}} \tag{7.a}$$

$$r = \sqrt{x^2+y^2+z^2} \tag{7.b}$$

$$\lambda = tan^{-1}\frac{y}{x} \tag{7.c}$$

where φ is geocentric latitude, co-latitude, θ is $90^o - \varphi$.

The relationship of the disturbing gradients given in eq. (1) with respect to spherical coordinates is given by (15). For example, the diagonal elements of Γ is given by

$$\Gamma_{zz} = \frac{\partial^2 T}{\partial r^2} \tag{8.a}$$

$$\Gamma_{yy} = \frac{1}{r}\frac{\partial T}{\partial r} + \frac{1}{r^2}\frac{\partial^2 T}{\partial \theta^2} \tag{8.b}$$

$$\Gamma_{xx} = \frac{cot\theta}{r^2}\frac{\partial T}{\partial \lambda} + \frac{1}{r}\frac{\partial T}{\partial r} + \frac{1}{r^2 sin^2\theta}\frac{\partial^2}{\partial \lambda^2} \tag{8.c}$$

By applying analytical derivatives to the equation (6), the disturbing gravity gradients are computed directly from EGM08 model. For example, Γ_{zz}, disturbing gradient is computed from equation 8.a,

$$\Gamma_{zz} = \frac{\partial^2 T}{\partial r^2} = \frac{GM}{a}\sum_{n=2}^{nmax}\sum_{m=-n}^{n}\frac{(n+1)(n+2)}{a^2}\left(\frac{a}{r}\right)^{n+3}\delta C_{nm}\overline{Y_{nm}}(\theta,\lambda) \tag{9}$$

Forward model generated curvature gradient is computed from

$$\Gamma_C = \left|\Gamma_{zz}^{(L)} + \Gamma_{zz}^{(R)}\right| \tag{10}$$

with $\Gamma_{zz}^{(L)}$ is the gradient generated by the density contrast on the left of the fault and $\Gamma_{zz}^{(R)}$is the gradients generated by the density contrast on the right of the fault [16].

$$\Gamma_{zz}^{(L)}(x,z) = 2G\Delta\rho^{(L)}\left(A^{(L)}cos\chi - D^{(L)}E\right)sin\chi$$

$$\Gamma_{zz}^{(R)}(x,z) = -2G\Delta\rho^{(R)}\left(A^{(R)}cos\chi - D^{(R)}E\right)sin\chi$$

where

$$A^{(L,R)} = \frac{F_2^{(L,R)}\theta_2^{(L,R)} - F_1^{(L,R)}\theta_1^{(L,R)}}{Esin\chi} - \frac{1}{2}ln\frac{G_1^{(L,R)}}{G_2^{(L,R)}}$$

$$D^{(L,R)} = \frac{E_2^{(L,R)}\theta_2^{(L,R)} - E_1^{(L,R)}\theta_1^{(L,R)}}{E^2 sin\chi}$$

$$\theta_{1,2}^{(L,R)} = tan^{-1}\frac{x - x_0 - z_{1,2}^{(L,R)}cot\chi}{z - z_{1,2}^{(L,R)}}$$

$$E = (x - x_0)sin\chi - zcos\chi$$

$$E_{1,2}^{(L,R)} = (x - x_0)sin\chi - z_{1,2}^{(L,R)}cos\chi$$

$$F_{1,2}^{(L,R)} = z - z_{1,2}^{(L,R)} + Ecos\chi$$

$$G_{1,2}^{(L,R)} = \left(x - x_0 - z_{1,2}^{(L,R)}\right)^2 + \left(z - z_{1,2}^{(L,R)}\right)^2$$

Monte Carlo inversion technique is called simulated annealing (SA) depending on Metropolis algorithm (1953) [17] that generates sequences of parameters from a Markov chain until it reaches equilibrium condition at a given temperature T. Then the temperature is reduced between subsequent Markov Chains. The SA algorithm can be considered as an implementation of Metropolis algorithm evaluated at decreasing values of the temperature. The equilibrium condition is identified by the Gibbs-Boltzman distribution. The Gibbs-Boltzman distribution defines the probabilities of being in a state $\hat{\xi}$ with energy $\phi(\hat{\xi})$ [18]

$$P\left(\xi = \hat{\xi}\right) \sim e^{-\frac{\phi(\hat{\xi})}{kT}} \tag{11}$$

where k is Boltzman constant, T is the temperature, ξ denotes current state of the system.

In optimization problem, energy of the state of the system is associated with a cost function. The cost function is defined as the sum of squared differences between differential curvature gradients, Γ_C, generated from EGM08 model and the corresponding gradients computed from the forward fault model.

$$\phi(\xi) = \sum_i\left(\Gamma_C^{EGM08}(x_i;\xi) - \Gamma_C^{model}(x_i;\xi)\right)^2 \tag{12}$$

The parameter vector ξ having size of $m \times 1$ includes the location of the fault, x_0 relative to northwestern end point of the profile, the dip angle of the fault, χ, and upper depths of the left and right layers, z_3, z_4 and x_i denotes the ith location point along the profile.

The aim is to find best estimated parameters that minimizes this cost function. This is achieved by stages of reducing temperatures sequentially. Each stage is performed to reach intermediate equilibrium and best parameters related to intermediate equilibrium. The equilibrium condition is reached when the average cost function does not change after a certain number of iterations performed at a fixed temperature.

At a given initial temperature, the SA algorithm starts some chosen initial arbitrary state ξ_0 within predefined search space

$$\xi_L^h < \xi < \xi_U^h \qquad h = (1, \ldots, m) \tag{13}$$

where $[\xi_L^h, \xi_U^h]$ is lower and upper search space boundaries for the parameters. And the corresponding cost function of the initial state $\phi(\xi_0)$ is computed. New state is generated from perturbing given initial state by

$$\xi_k^h = \xi_j^h + r \cdot \Delta\xi^h \quad subject\ to\ \ \xi_L^h < \xi < \xi_U^h \tag{14}$$

where r is a randomly generated number from a uniform distribution between [-1,1] and $\Delta\xi^h$ is the hth component of defined step length factor. The corresponding cost function of the next state is computed. At each step in the chain, new candidate state is accepted as current state with probability one if $\Delta\phi = \phi_k - \phi_j \leq 0$. If $\Delta\phi > 0$, then the new state is accepted with probability according to metropolis acceptance ratio [19]

$$\alpha = min\left(1, \frac{P_k}{P_j}\right) = min\left(1, e^{-\frac{\phi(k)-\phi(j)}{T}}\right) \quad (15)$$

where P_j is the probability of the state, ξ_j, P_k is the corresponding probability of the consequent state of the system. This procedure is repeated until there is no change in the cost function.

3. Results and Dicussion

The study area, southwest side of the Thrace basin, is shown in Figure 2a. [7] describe several fault zones in the region, Pehlivankoy-Yenicegore fault zone, Karabürçek-Ibriktepe fault zone and Karaidemir-Karatepe fault zone trending NE-SW and Subasi-Kozyoruk fault zone trending NW-SE. It is interested in estimating parameters of two faults which are located in east side of Karabürçek-Ibriktepe fault zone and south side of Karaidemir-Karatepe fault zone. (Figures 4a-4b). Faults lying east side of Karabürçek-Ibriktepe fault zone are represented several parallel segments lying in the area of 10 km wide between Harmanli-Beykonagi-Karabürçek. East side segments of Karabürçek-Ibriktepe fault zone which consists of two step faults lie between Gazimehmet and Beykonagi. From seismic studies done by [7], the dip angle of the fault residing in southeast side of these two step faults was reported between 73 and 81°. Karaidemir-Karatepe fault zone also contains several fault segments, one of which lies between Esetce and Sarpdere. Field observations performed by [7] on the southwest side of this fault indicate dip angle of 76°. It is tried to model these two faults and estimate their parameters from the curvature gravity gradients.

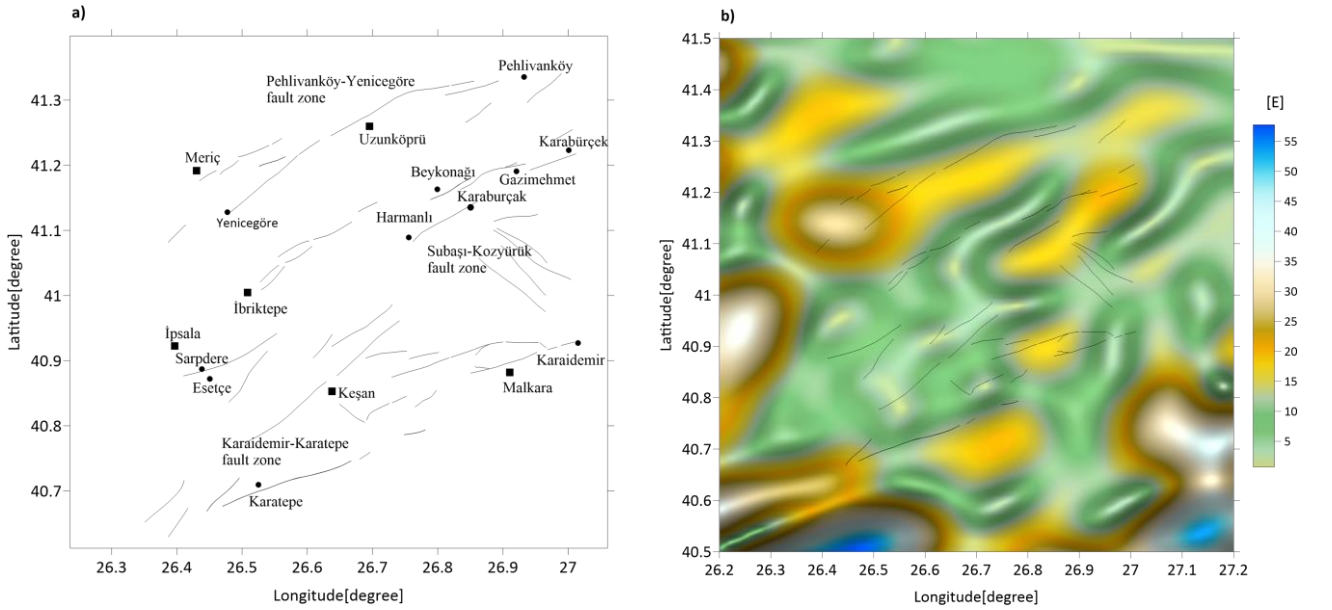

Figure 2. a) Faults in the southwest of the Thrace basin adapted from [7]. b) Differential curvature gradients , Γ_C computed from EGM08 model up to $n_{max} = 1728$. Fault lines are transcribed from Figure 2a.

Full resolution of EGM08 model up to harmonic degree 2160 represents complete gravitational field including the effect of topography. Figures 3a-b indicate topography map of the region computed from SRTM (Shuttle Radar Topography Mission) data and Bouguer gravity anomalies Δg_B computed from EGM08 model and DTM2006 spherical harmonic topographic expansion model [10]. Free air gravity anomaly is given by [14]

$$\Delta g(r,\theta,\lambda) = \\ = \frac{GM}{a^2}\sum_{n=2}^{nmax}(n-1)\left(\frac{a}{r}\right)^{n+1}\sum_{m=-n}^{n}\delta C_{nm}\overline{Y_{nm}}(\theta,\lambda) \quad (16)$$

The Bouguer gravity anomaly is defined by $\Delta g_B = \Delta g - 2\pi\rho G h$, where density is $\rho = 2.67 g/cm^3$ and h is topographic height generated from DTM2006.

Figures 4a-b) illustrate differential curvature gradients, Γ_C computed from EGM08 model using equation 5 for two different resolutions. One way to remove topography is to use lower resolution of the EGM08 model. Lower resolutions of EGM08 model up to maximum degree and order 1728 and 1440 are used to estimate fault parameters in this study. The relationship between n_{max} and resolution $\Delta\phi$ being half-wavelength, is given by $n_{max} = \pi R/\Delta\phi$ at the equator. In the study area, east-west resolution of EGM08 model for n_{max}=1728 is about 8.4 km. and n_{max}=1440 is about 10.5km.

As can be seen from Figures 4a-b, fault segment of Gazimehmet-Beykonagi is not completely visible in the lower resolution of the EGM08 model. Therefore, this fault parameters are not tried to estimate from lower resolution of the EGM08 model. Cross-strike profiles and faults used in the estimation process are shown in Figures 4a-b.

Parameters of one fault segment of Gazimehmet-Beykonagi and the fault lying between Esetce and Sarpdere are tried to estimate from curvature gradients along profiles, EE' and AA' , which are computed from EGM08 model up to maximum harmonic degrees, n_{max}=1728 and n_{max}=1440. The length of the profiles, EE' and AA' is 26.2 km and 14.8 km, respectively.

For implementation of the optimization, search spaces of the fault parameters have to be defined. For this purpose, fault geometry and geologic information of the basin have been considered. Search space of the location parameter is set to the length of the data profiles, $EE'$and AA'. The search spaces of the other parameters are determined from based on some known fault data, geologic information and previous seismic studies. According to [5], maximum thickness of the basin reaches up to 9 km. [7] reported that the dip angle of the faults lying in the southwest part of the basin is between 60-83°. Therefore, the search spaces for the other parameters are defined as in Table 1.

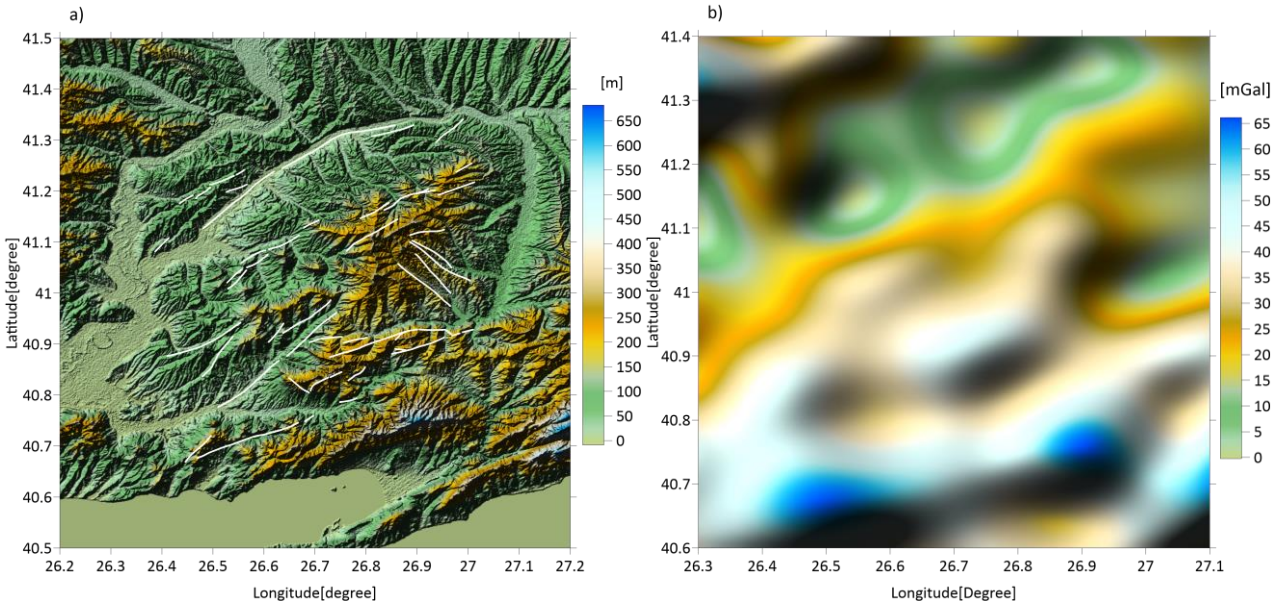

Figure 3. a) Topography map of the Thrace basin. Faults are transcribed from figure 2a. b) Bouguer gravity anomaly map, Δg_B generated from EGM08 and DTM2006 models.

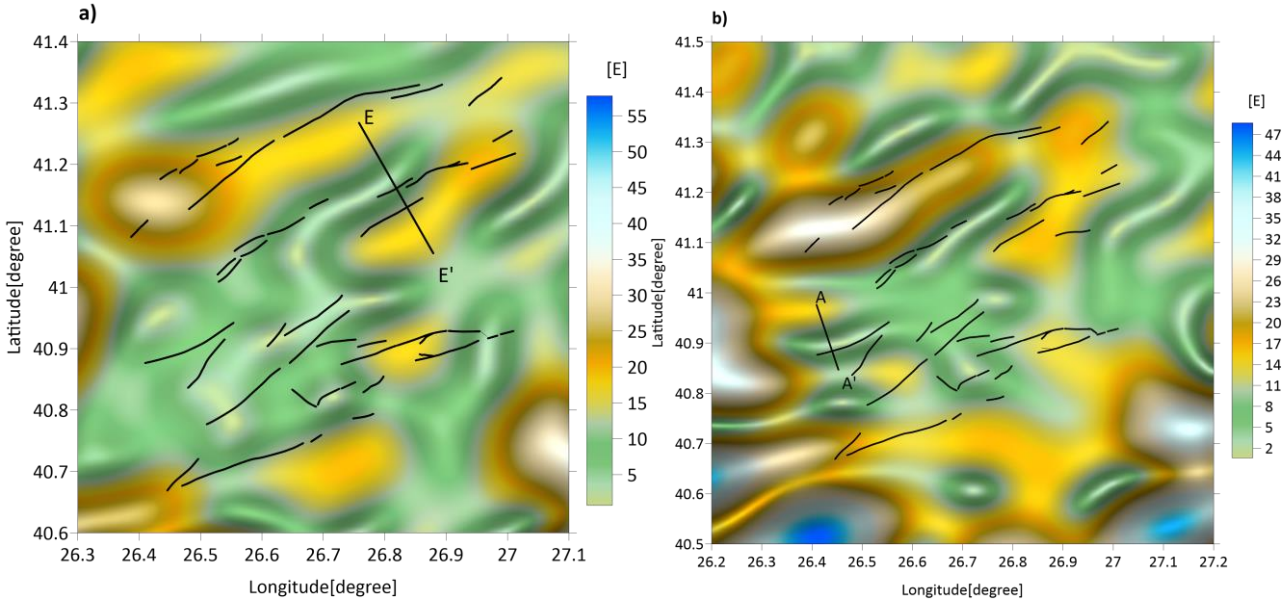

Figure 4. a) Profile EE' along the fault and differential curvature gradient map generated from EGM08 model up to degree n_{max} =1728. b) Profile AA' along the fault and differential curvature gradient, Γ_C map generated from EGM08 model up to degree n_{max} =1440.

Table 1. Upper ξ_U and lower ξ_L boundaries of search space for the parameters.

Parameters	Profile EE'	Profile AA'
x_0 [km]	$0 \le x_0 \le 17$	$0 \le x_0 \le 15$
χ[°]	$10 \le \chi \le 90$	$10 \le \chi \le 90$
z_3 [km]	$-12 \le z_3 \le -0.5$	$-12 \le z_3 \le -0.5$
z_4 [km]	$-10 \le z_4 \le -0.5$	$-7 \le z_4 \le -0.5$

In this algorithm, length of the Markov chain is a fixed number defined by user. The length of the Markov chain is defined by $n = N_T \cdot L_\delta$. After $L_\delta \cdot m$ iterations, the step length is dynamically adjusted N_T times so that 40-60% of perturbed states are accepted [21]. After n realizations of m Markov chains, the temperature is reduced. Temperature reduction is given by $T_{k+1} = \tau \cdot T_k$, where, τ is temperature reduction rate between [0,1]. Reasonable slow cooling rate could be chosen between 0.5 and 0.95.

Figure 5 shows simulated differential curvature gradient observations along the profile EE' based on forward model given in Figure 1. Nominal parameter values of the forward model are defined by, x_0 =13 km, χ =75°, $z_1 = -12$ km, $z_2 = -10$ km, $z_3 = -5$ km, $z_4 = -3$ km, $\Delta\rho_1$ =500 kg/m³, $\Delta\rho_2$ =100 kg/m³. It is assumed that observation profile is at zero elevation (z=0).

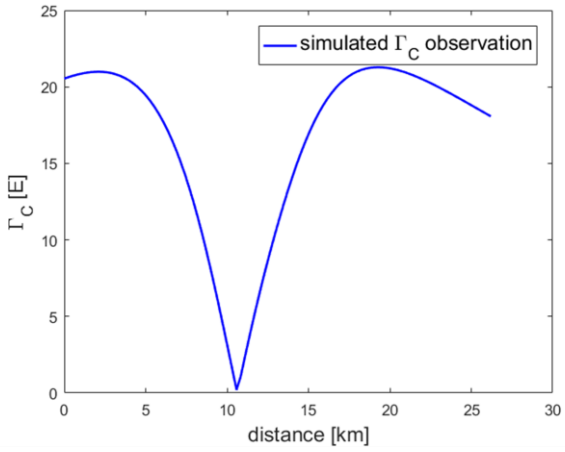

Figure 5. Simulated differential curvature gradient, Γ_C observation (sought signal).

In this case, the length of the Markov Chain is set to $n = N_T \cdot L_\delta$ =20·20=400. The lower ξ_L and upper ξ_U boundaries of the parameter space are defined by

$0 \leq x_0 \leq 25$ km; $10 \leq \chi \leq 90^o$;

$-12 \leq z_3 \leq -0.5$ km; $-10 \leq z_4 \leq -0.5$ km

$-15 \leq z_1 \leq -8$ km; $-12 \leq z_2 \leq -8$ km

After several test run of the SA algorithm, initial temperature is set to T=1000 and the temperature reduction rate is set to τ=0.85. Convergence rate of the parameters based on different initial parameter values, different initial temperatures and temperature reduction rates are given in Figure 6. In addition, to test the success of the SA optimization on estimating fault parameters, some noise added to the simulated signal given in Figure 5. The results are provided in Table 2. As the noise level of the simulated signal increases, estimated parameters in comparison to real model parameter values deteriorate. For the last test case, the initial temperature is T =100000, and N_T=50. The lower depth parameter estimate, z_2 reaches its allowed search limit while the other parameter estimates are reasonable in comparison to real fault model parameters.

Table 2. The fault parameter estimates for the profile, EE′ .

Noise level	x_0 [km]	χ [°]	z_3 [km]	z_4 [km]	z_1 [km]	z_2 [km]	Cost function [E^2]
0E	13.00	75.0	-5000	-3000	-12000	-10000	3.030×10^{-7}
0.1E	13.21	73.74	-4978	-2935	-12000	-10008	8.48×10^{-1}
0.5E	13.65	71.28	-4875	-2676	-12320	-12000	21.24

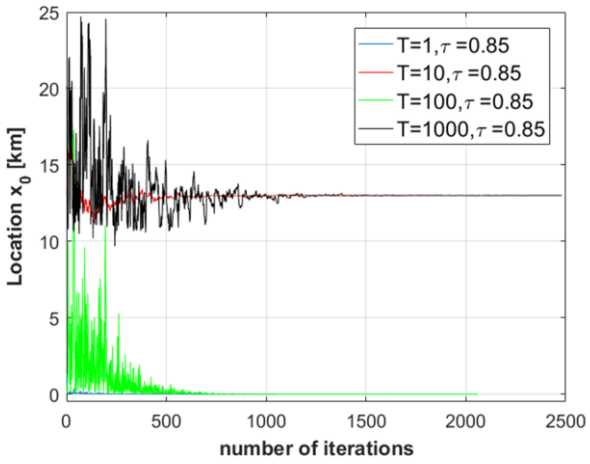

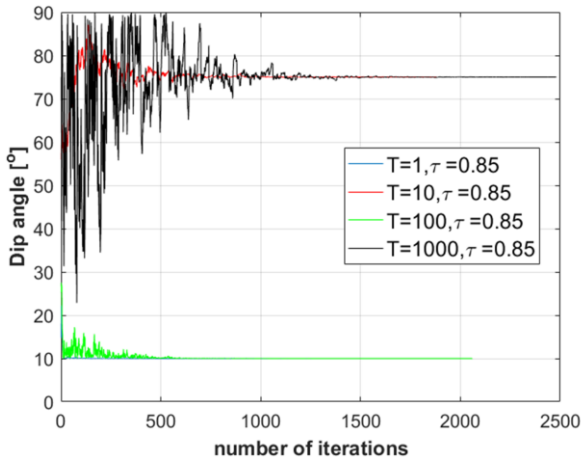

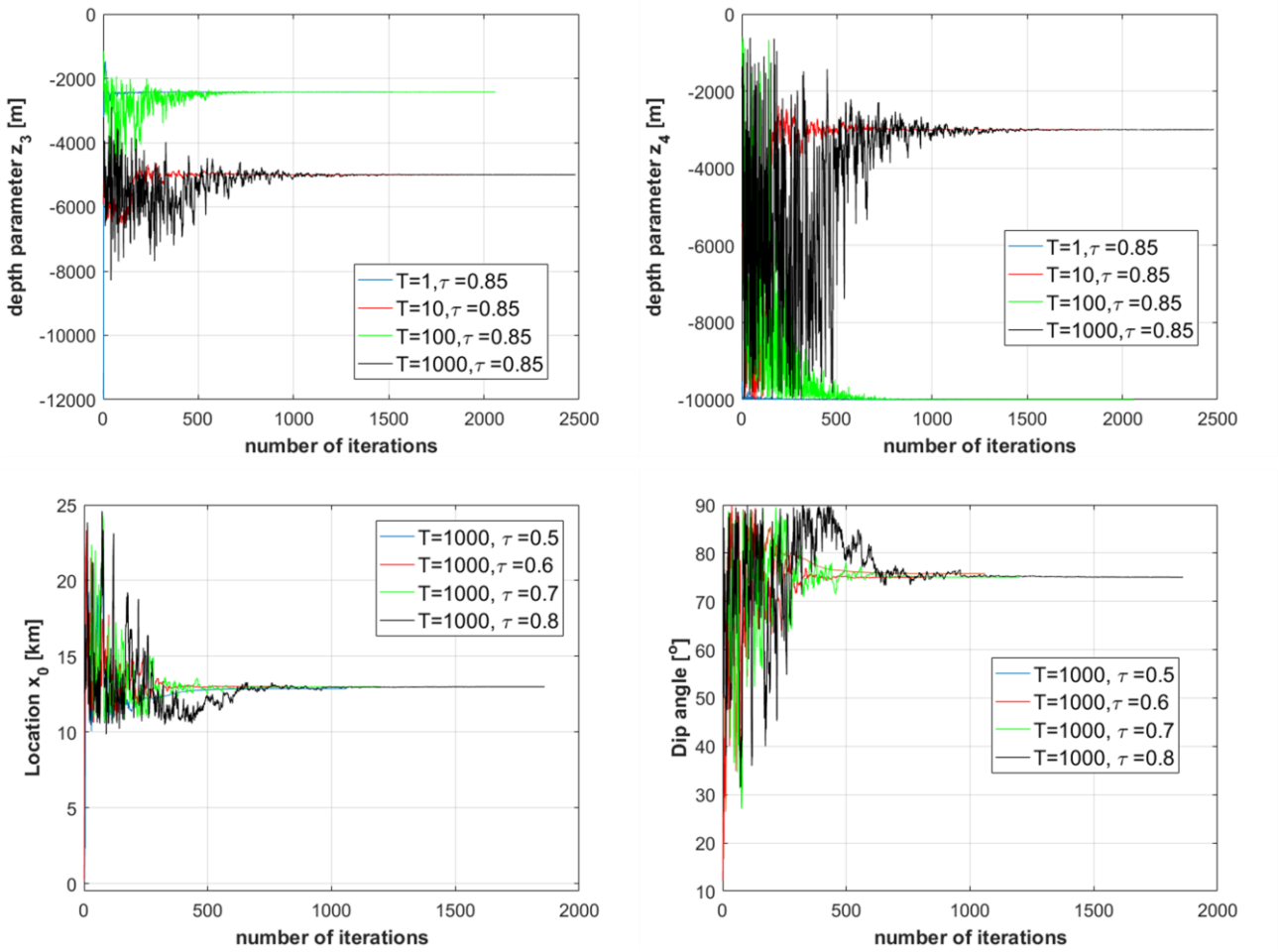

Figure 6. Convergence rates of the fault parameters for different initial temperatures and temperature reduction rates.

Similar analyses have been performed for real data case. In this case, the length of the Markov chain is $n = N_T \cdot L_\delta$ =20 · 20=400. The lower ξ_L and upper ξ_U boundaries of the parameter space are given in Table 1. The initial temperature is set to T=10000 and temperature reduction rate is set to τ=0.85 after several runs of the SA algorithm. Convergence rates of the parameters based on different initial temperatures, different initial parameters and fixed $\tau = 0.85$ are given in Figures 7a-b for two profiles.

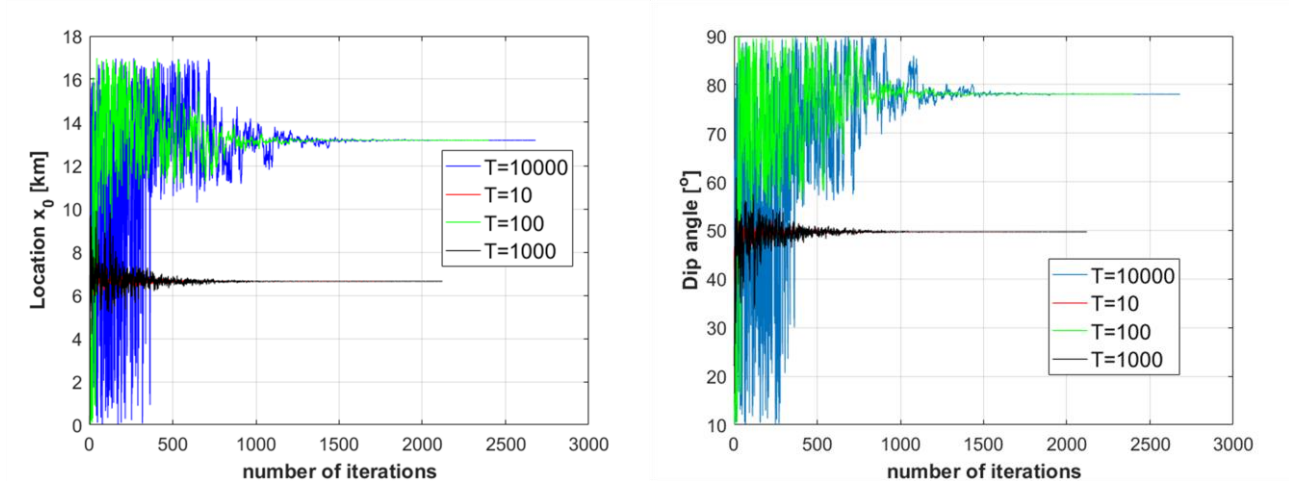

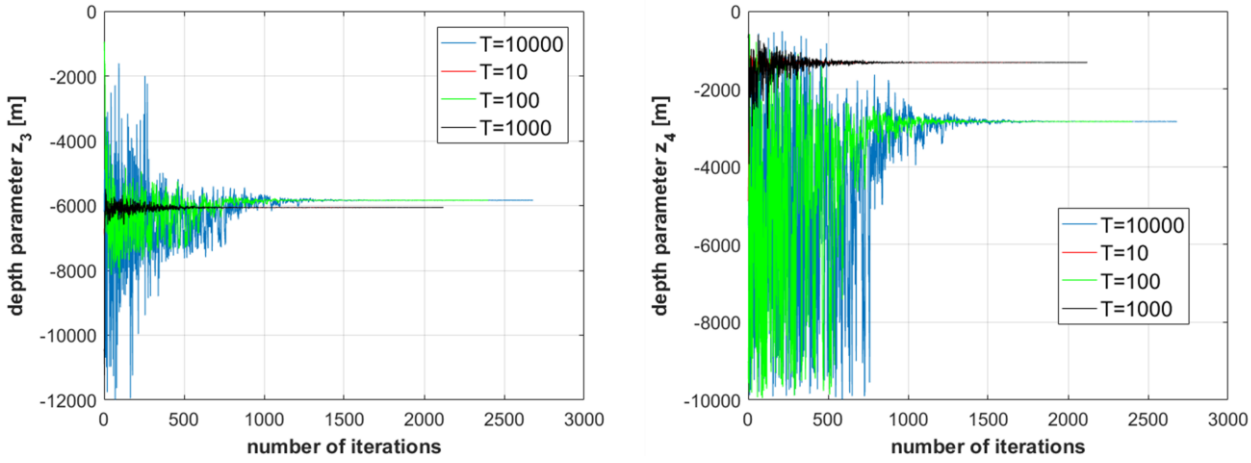

Figure 7. a) Convergence rates of the parameters for different initial temperatures using profile EE' for case 1

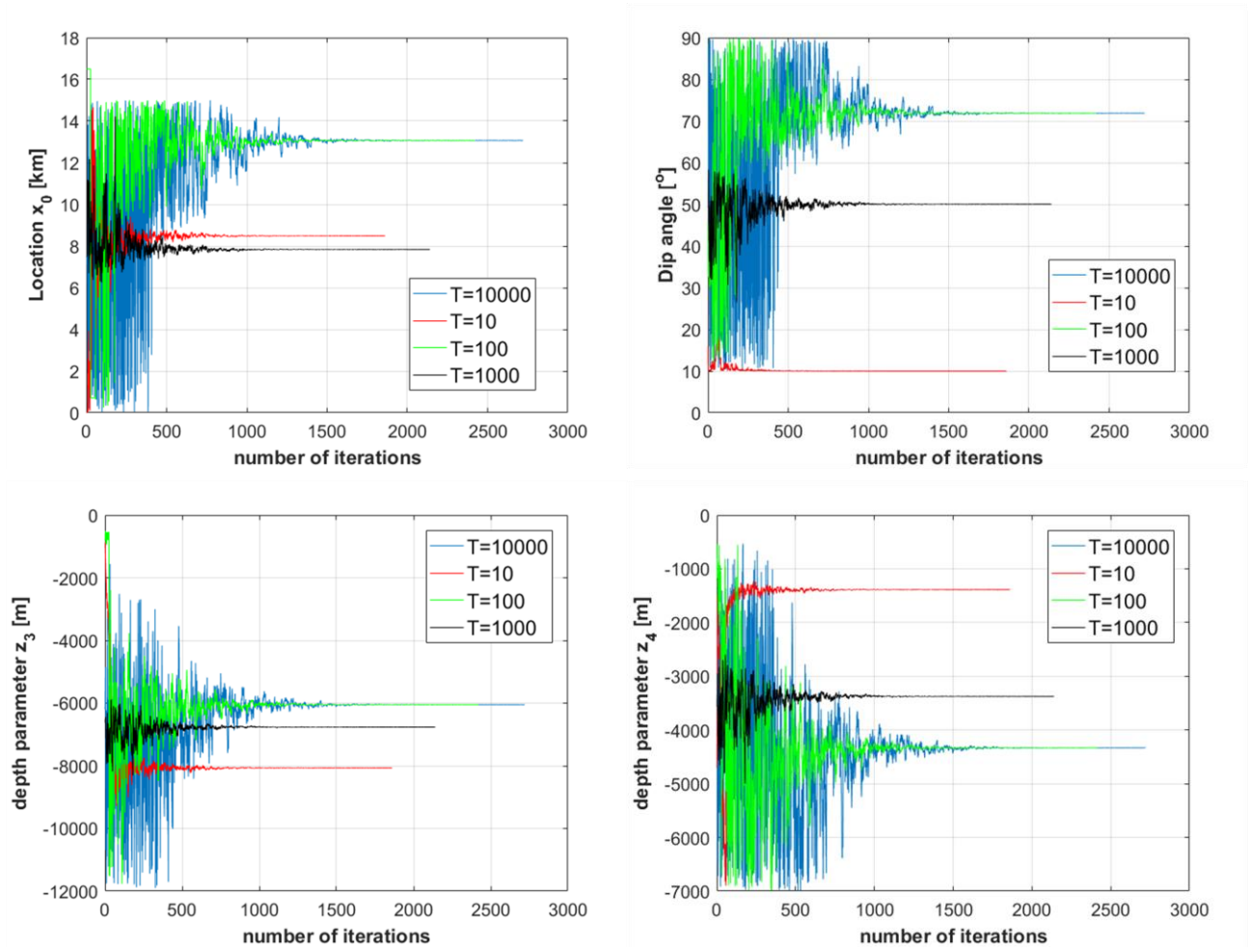

Figure 7. b) Convergence rates of the parameters for different initial temperatures using profile AA' for case 2

Estimated parameters of the faults are listed in Table 3. These results are obtained at least 10 independent runs of the SA algorithm. Estimated dip angles are found to be consistent with seismic studies done by [7]. While estimated location of the fault along profile EE' (Figure 8a) agrees with the seismically defined location of the fault, there is a difference between estimated and mapped location of the fault along profile AA' (Figure 9a). Two reasonable solutions are obtained from the profile, EE'. According to stratigraphic cross section of the area made by [20], either side of the fault is set to the different density contrasts. It is noted that changing the density contrasts does not lead to significant change on the dip angle and the location estimates, but results in the left upper depth estimate to be adjusted to a lower depth value. From Bouguer gravity anomaly map, the area has the

lowest positive anomaly, probably due to deeper geologic structures. According to [5], thickness of the area is around 7km which agrees with the fault geometry found in case I. A plot that compares the fitted fault model with EGM08 profile for case I is given in Figure 8b.

Similarly, two reasonable solutions are obtained from the profile, AA'. In this case, the dip angle estimate is computed to be around 72^o.Similarly, changing the density contrasts does not lead to significant change on the dip angle and the location estimates, but results in the upper depth of the left layer to be adjusted to a lower depth value. From stratigraphic cross section [20], it is inferred that the density contrasts for left and right layers of the fault can be set to different values. From previous studies [5-9], it is inferred that the thickness of the area is around 4-5km. It is concluded that case II agrees with the geologic information provided in the area and is considered as an appropriate solution for this profile. A plot that compares fitted fault model with EGM08 profile for case II is given in Figure 9b.

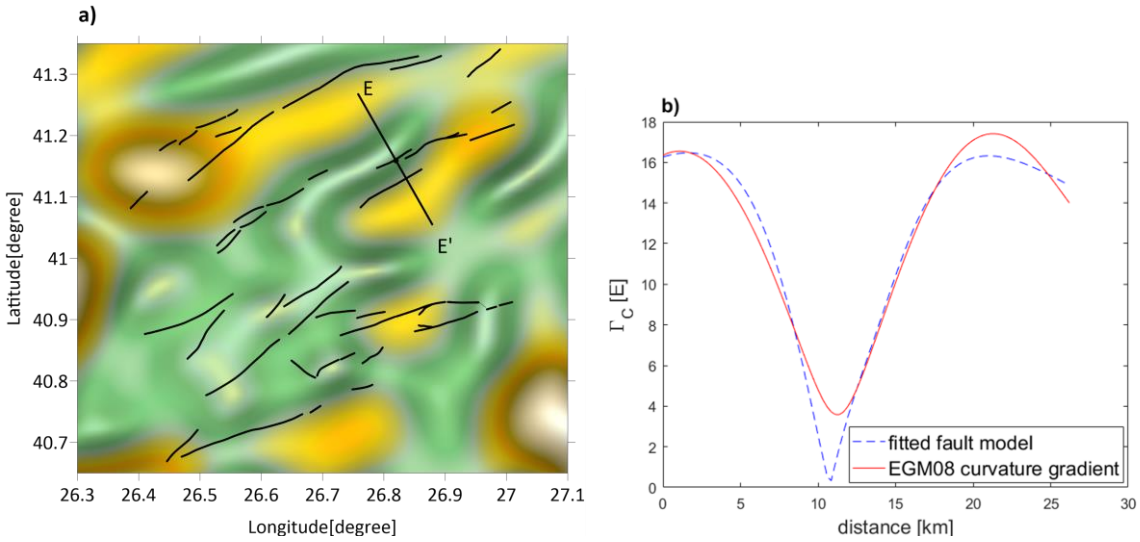

Figure 8. a)The location estimate is shown black dot along profile EE' with EGM08 differential curvature gradient map, Γ_C, (n_{max} =1728). b) A comparison of fitted fault model with EGM08 differential curvature gradients along profile EE' .

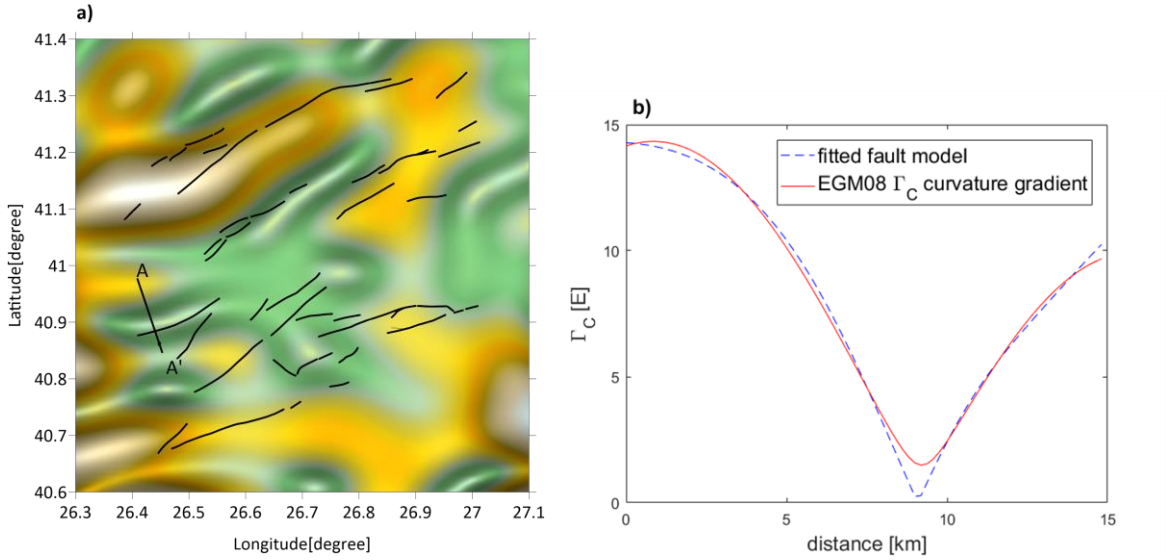

Figure 9. a) The location estimate is shown black dot along profile AA' with EGM08 differential curvature gradient map, Γ_C, (n_{max}=1440). b) A comparison of fitted fault model with the EGM08 differential curvature gradients along profile AA'.

Table 3. Parameter estimates along profiles, EE' and AA'. Bold values are not estimated.

Profile	Case	x_0 [km]	χ [°]	z_3 [km]	z_4 [km]	z_1 [km]	z_2 [km]	$\Delta\rho_1$ [kg/m³]	$\Delta\rho_2$ [kg/m³]	Cost function [E²]
EE'	I	13.17	78.04	-5838	-2839	**-12000**	**-10000**	**500**	**100**	90.054
	II	13.29	77.52	-2920	-2720	**-12000**	**-7000**	**500**	**500**	85.338
AA'	I	12.98	72.22	-5026	-4361	**-12000**	**-7000**	**500**	**500**	9.909
	II	13.07	71.88	-6049	-4334	**-12000**	**-7000**	**500**	**300**	9.660

Finally, all model parameters are estimated from two profiles. In this case, the length of the Markov chain is $n = N_T \cdot L_\delta$=60·20=1200. The initial temperature is T=100000 for case I. Upper ξ_U and lower ξ_L boundaries of the search space are defined by

$0 \le x_0 \le 17$ km; $10 \le \chi \le 90^o$;

$-10 \le z_3 \le -0.5$ km; $-7 \le z_4 \le -0.5$ km

$-15 \le z_1 \le -12$ km; $-13 \le z_2 \le -8$ km

$100 \le \Delta\rho_1 \le 600$kg/m³;$100 \le \Delta\rho_2 \le 500$ kg/m³.

The results are listed in Table 4. As can be seen from Table 4, the SA algorithm is not able to find global minimum of the cost function in case I. In case II, the solution is not robust since different initial parameter values lead to different estimates but converge to the same cost function.

Table 4. All fault parameter estimates using SA optimization along profiles, EE' and AA'.

Profile	Case	x_0 [km]	χ [°]	z_3 [km]	z_4 [km]	z_1 [km]	z_2 [km]	$\Delta\rho_1$ [kg/m3]	$\Delta\rho_2$ [kg/m3]	Cost function [E²]
EE'	I	13.45	77.67	-1742	-1569	-14300	9906	553.1	500	60.092
	II	15.00	70.13	-6778	-6996	-13610	-9452	566.5	477.7	70.116
AA'	I	14.74	66.80	-7491	-5088	-12830	-7352	600	323	7.79
	II	14.81	66.58	-7351	-5270	-12820	-7307	600	397.6	7.80

4. Conclusions

This study presents a gravity gradient analysis of the Thrace basin based on high resolution EGM08 data. Curvature differential gradient is used in modelling faults since it identifies lineaments of linear features in the gravitational field and are also useful for delineating geologic structures. Due to the near surface inhomogeneities, truncated EGM08 data are used to compute the fault parameters in the region. It is concluded that the dip angle estimates of the faults are found to be high angle which agree with previously conducted geologic studies. The location of the fault lying southeast side of Gazimehmet-Beykonagi is consistent with the seismically mapped fault location. As indicated in seismic studies, the fault lying southwest side of the Karaidemir-Karatepe fault zone are found to be having south block rising dip-slip fault. However, the location of the fault is found to be different from seismically mapped location. This could be due to geologic complexity that are not included in the fault model. However, according to seismic studies, between Ipsala, Kesan and Sahin, the slickenlines of the faults are not exposed to the surface. The fault surfaces in the region are either deteriorated or buried in Ergene formation.

To estimate the location, the dip angle and the upper depth parameters, some constraints are added to the SA inversion by fixing the density contrasts and the lower depth parameters based on seismic studies. It is noted that the fault parameters are estimated from using only gravity gradient data which is known to be an ill-posed problem. In addition to gravity gradient data, other seismic, magnetic or geodetic data can be incorporated into inversion problem to improve solutions on these parameter estimates.

Ethics committee approval and conflict of interest statement

This article does not require ethics committee approval.

This article has no conflicts of interest with any individual or institution.

Acknowledgment

The author gratefully thanks two anonymous reviewers for helping to improve the manuscript.

Author Contribution Statement

S. Uzun conceptualized the manuscript, wrote original draft, carried out numerical experiments, revised the manuscript and approved final version of the manuscript.

References

[1] Perinçek, D. 1991. Possible Strand of the North Anatolian Fault in the Thrace Basin, Turkey-An Interpretation, The American Association of Petroleum Geologists Bulletin, V. 75, 241-257.

[2] Turgut, S., Türkarslan, M. and Perinçek, D. 1991. Evolution of the Thrace Sedimentary basin and its hydrocarbon prospectivity, in generation, accumulation and production of Europe's hydrocarbons, special publication of the European Association of Petroleum Geoscientists, Oxford University Press, No.1, 415-437.

[3] Perinçek, D., Ataş, N., Karatut, Ş. and Erensoy, E. 2015. Geological Factors controlling potential of Lignite Beds within, the Danişmen Formation in the Thrace Basin, Bulletin of the Mineral Research and Exploration, issue. 150, 79-110.

[4] Coşkun, B. 2000. Influence of the Istranca-Rhodope Massifs and Strands of the North Anatolian Fault on oil potential of Thrace Basin, NW Turkey, Journal of Petroleum Science and Engineering, V.27, 1-25.

[5] Siyako, M. and Huvaz, O. 2007. Eocene Stratigraphic evolution of the Thrace Basin, Turkey, Sedimentary Geology, V.198, 75-91.
[6] Demir, D., Bilim, F., Aydemir, A. and Ates, A. 2012. Modelling of Thrace Basin, NW Turkey using gravity and magnetic anomalies with control of seismic and borehole data, Journal of Petroleum Science and Engineering, V.86-87. 44-53. DOI:10.1016/j.petrol.2012.03.013
[7] Elmas, A., Yılmaz, I and Kırcı, E. 2008. Güneybatı Trakyada Neojen-Erken Kuvaterner döneminde etkili olan yapısal özelliklerin araştırılması, The Scientific and Technical Research Council of Turkey, Ankara, Report No:105Y299, p.157.
[8] Aydogan, D., Pinar, A., Elmas, A., Bal, O. T. and Yuksel, S. 2013. Imaging of subsurface lineaments in the southwestern part of the Thrace Basin from gravity data: Earth Planets Space, V.65, 299-309. DOI: 10.5047/eps.2012.08.014
[9] Tekkeli, A. B. 2013. Modeling of Gravity Anomalies using Genetic and Particle Swarm Algorithms, PhD thesis, Istanbul Technical University, p.147.
[10] Pavlis, N.K., Holmes, S.A., Kenyon, S.C., Factor, J.F. 2012. The development and evaluation of Earth Gravitational Model (EGM2008): Journal of Geophysical Research, V.117, B04406, DOI: 10.1029/2011JB008916.
[11] Jekeli, C. 2017. Spectral Methods in Geodesy and Geophysics, Taylor and Francis, p.310.
[12] Hofmann-Wellenhof, B. and Moritz, H. 2005. Physical Geodesy, Springer Verlag, Berlin, p.397.
[13] Heiland, C.A.1940. Geophysical Exploration, Prentice-Hall, New York.
[14] Jekeli, C. 2015. Potential theory and static gravity field of the Earth. Treatise on Geophysics, 2nd edition, G Schubert (ed.), Vol. 3, 9-35. Elsevier Publ., Oxford.
[15] Reed, G.B. 1973. Application of kinematical geodesy for determining the short wave length components of the gravity field by satellite gradiometry. Report no.201, Department of Geodetic Science, Ohio State University, Columbus, Ohio.
[16] Uzun, S. (2013). Estimating parameters of subsurface structures from airborne gravity gradiometry data using a Monte-Carlo Optimization Method. Report no.506, Geodetic Science, Ohio State University, Ohio.
[17] Metropolis, N., Rosenbluth, A.W., Rosenbluth, M.N. and Teller, A.H. 1953. Equation of state calculations by fast computing Machines: The Journal of Chemical Physics, V.21, no.6, 1087-1092.
[18] Geman, S. and Geman, D. 1984. Stochastic relaxation, Gibbs distributions and the Bayesian restoration of images: IEEE Transactions on Pattern Analysis and Machine Intelligence, V.6, no.6, 721-741.
[19] Chib, S. and Greenberg, E. (1995): Understanding the Metropolis-Hastings Algorithm, The American Statistician, V.49, no.4, 327-335.
[20] Elmas, A and Şengül, A. 2013. Miocene formations and NE- trending right-lateral strike-slip tectonism in Thrace, Northwest Turkey: Geodynamic Implications, International Geology Review, V.55, no.6, 705-729. DOI: 10.1080/00206814.2012.734041
[21] Corana, A.M., Marchesi, M., Martini, C. and Ridella, S.1986. Minimizing Multimodal Functions of continuous Variables with the Simulated Annealing, ACM Transactions on Mathematical Software, V.13, 262-280.